Supporting Information of

Atomic Layer Deposition onto Thermoplastic Polymeric Nanofibrous Aerogel Templates for Tailored Surface Properties

Jianwei Lu[1,2,3], Yi Li[3,4], Wei Song[1], Mark D. Losego[3,4], Rebhadevi Monikandan[5], Karl I. Jacob[2,3,4]*, Ru Xiao[1]*

1. State Key Laboratory for Modification of Chemical Fibers and Polymer Materials, College of Materials Science and Engineering, Donghua University, Shanghai 2016, P. R. China

2. School of Materials Science and Engineering, Georgia Institute of Technology, Atlanta, Georgia 30332

3. The Georgia W. Woodruff School of Mechanical Engineering, Georgia Institute of Technology, Atlanta, Georgia 30332

4. Renewable Bioproducts Institute, Georgia Institute of Technology, Atlanta, Georgia 30332

5. Materials Characterization Facility, Georgia Institute of Technology, Atlanta, Georgia 30332, United States

Correspondence to: Karl I. Jacob (E-mail: karl.jacob@mse.gatech.edu)
Ru Xiao (E-mail: xiaoru@dhu.edu.cn)

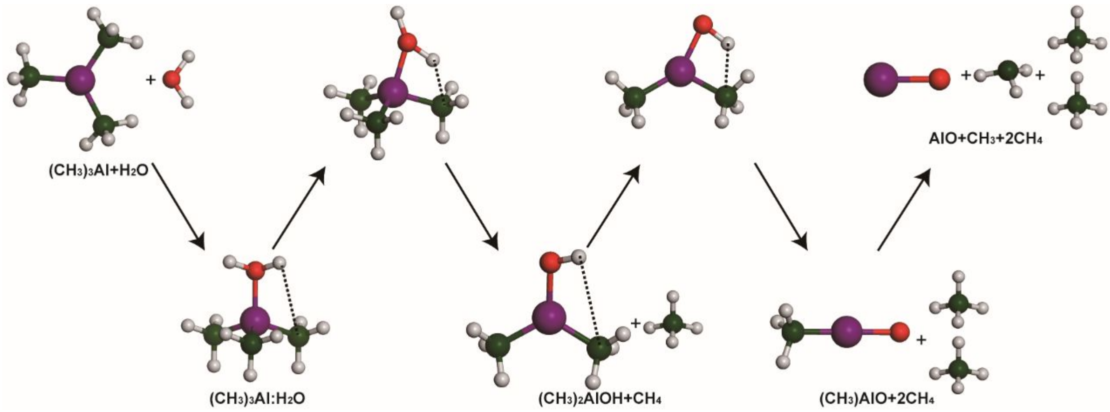

Figure S1 The reaction mechanisms of trimethylaluminum (TMA) with water.[1]

The reaction mechanisms of TMA with water were written as follows:

$(CH_3)_3Al + H_2O \rightarrow (CH_3)_3Al : H_2O$

$(CH_3)_3Al : H_2O \rightarrow (CH_3)_2AlOH + CH_4$

$(CH_3)_2AlOH \rightarrow (CH_3)AlO + 2CH_4$

$(CH_3)AlO \rightarrow AlO + CH_3 + 2CH_4$

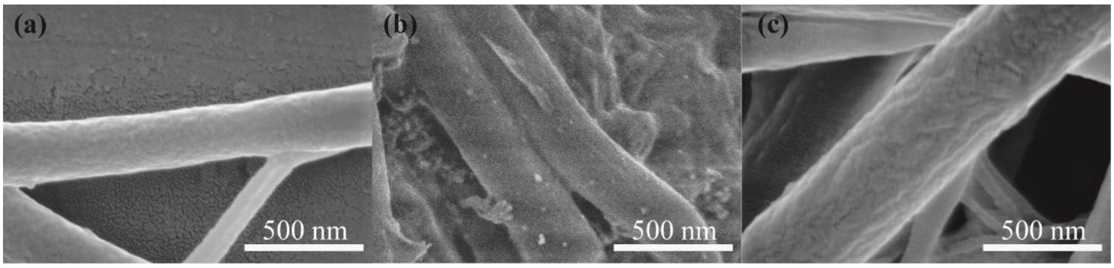

Figure S2 FE-SEM micrographs of surface's EVOH nanofibers with (a) 0, (b)6 and (c) 100 ALD cycles, the surface variation of EVOH nanofibers on the surface of aerogels was observed, demonstrating Al_2O_3 particles could uniformly deposit both the exterior and interior of the aerogels.

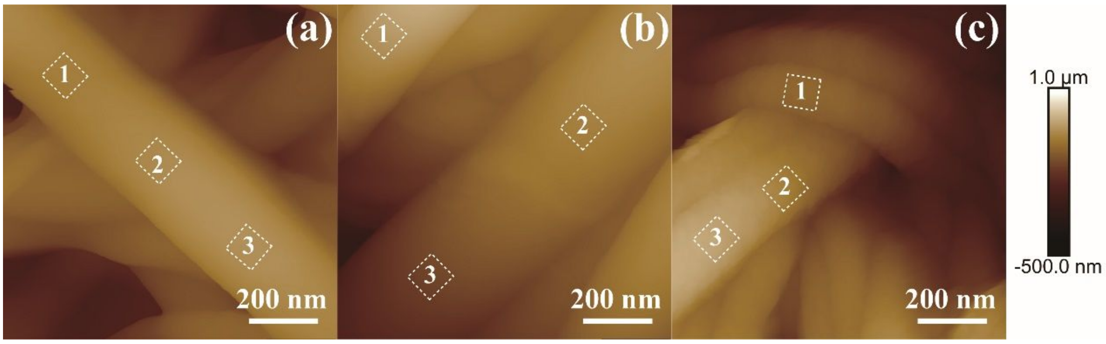

Figure S3 AFM images of EVOH nanofibers in (a) 0, (b) 6 and (c) 100cy-ALD aerogels, demonstrating the surface roughness variations of nanofibers with different ALD cycles. The surface roughness of EVOH nanofibers increased after 6 ALD cycles. While the surface roughness of EVOH nanofibers decrease, with ALD cycles continued increase to 100.

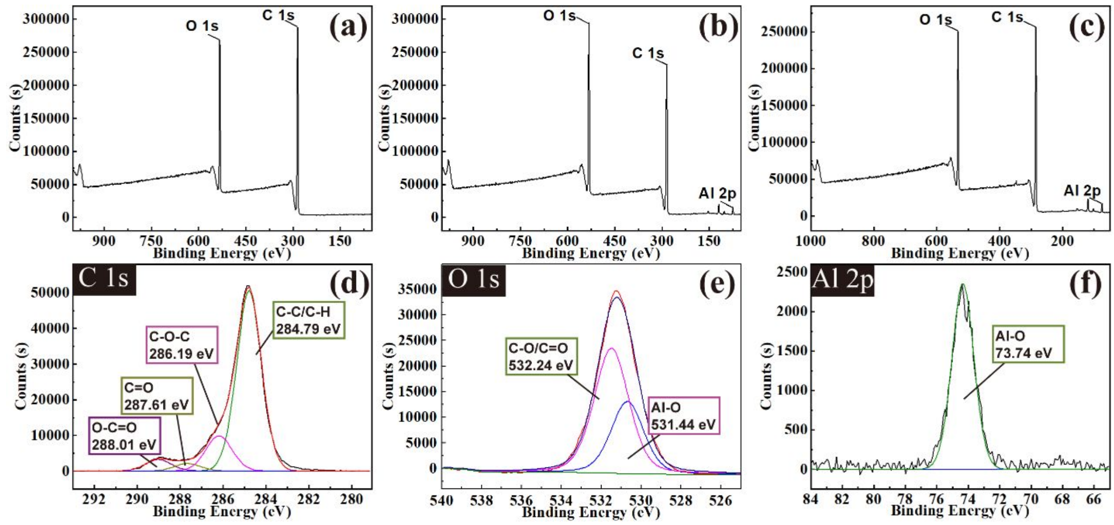

Figure S4 XPS survey scans of (a) 0, (b) 1 and (c) 6cy-ALD aerogels, XPS spectra for (d) carbon, (e) oxygen and (f) aluminum for 6cy-ALD aerogels, demonstrating the successful deposition of Al_2O_3 on the surface of aerogels after 6 ALD cycles.

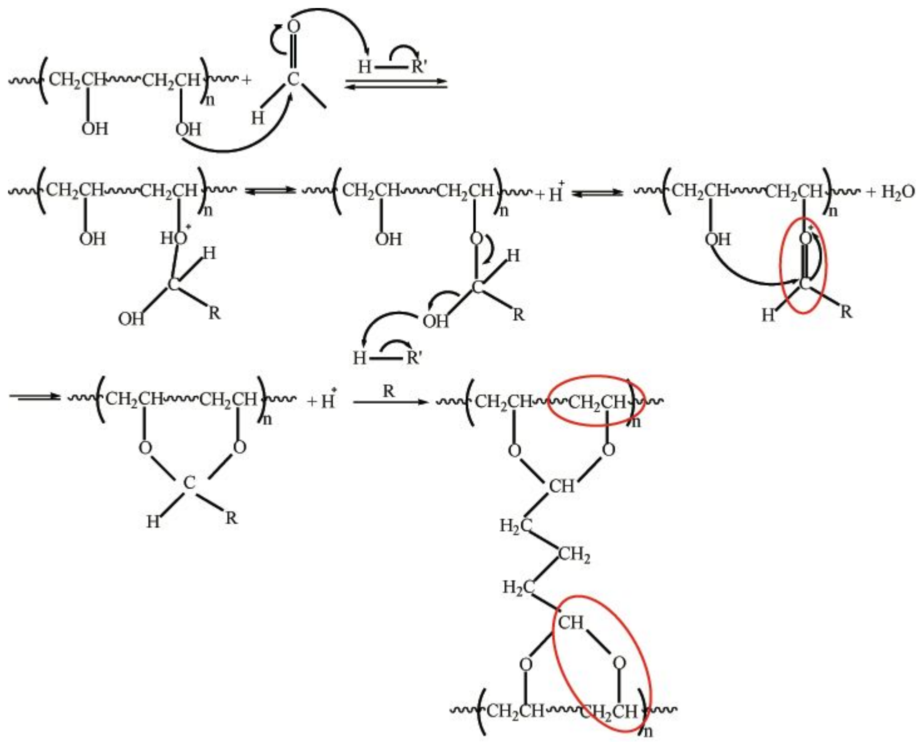

Figure S5 Mechanism of cross-linking between EVOH nanofibers and GA, demonstrating the formation of C-C, C-O-C and C=O.

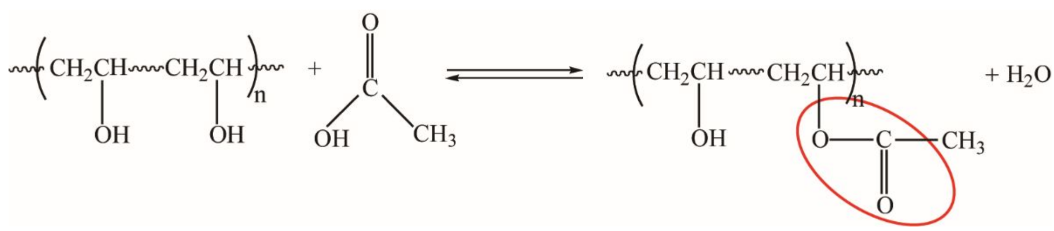

Figure S6 Mechanism of esterification reaction of EVOH nanofibers and acetic acid, demonstrating the formation of O-C=O.

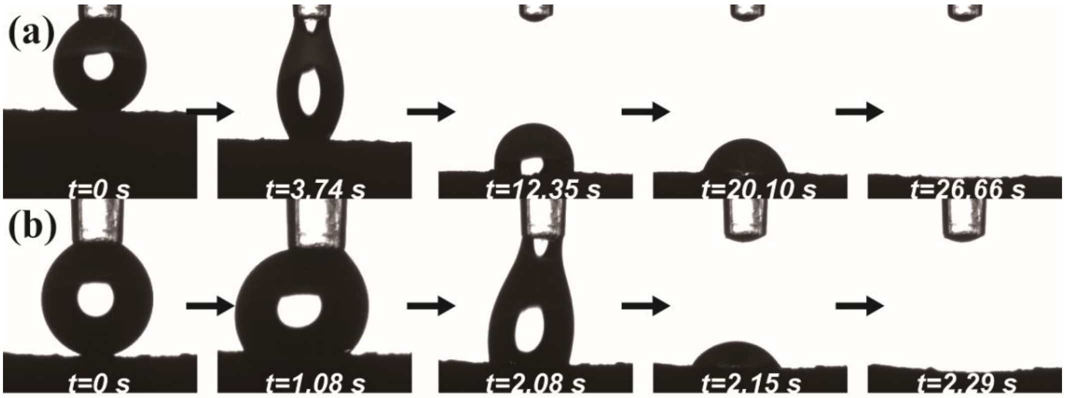

Figure S7 Photographs show the dynamic water contact angles of (a) 0 and (b) 8cy-ALD aerogels, the variation of water droplets on the surface of aerogels was observed. The water droplets were absorbed quickly by 0 and 8cy-ALD aerogels, demonstrating their hydrophilic surface.

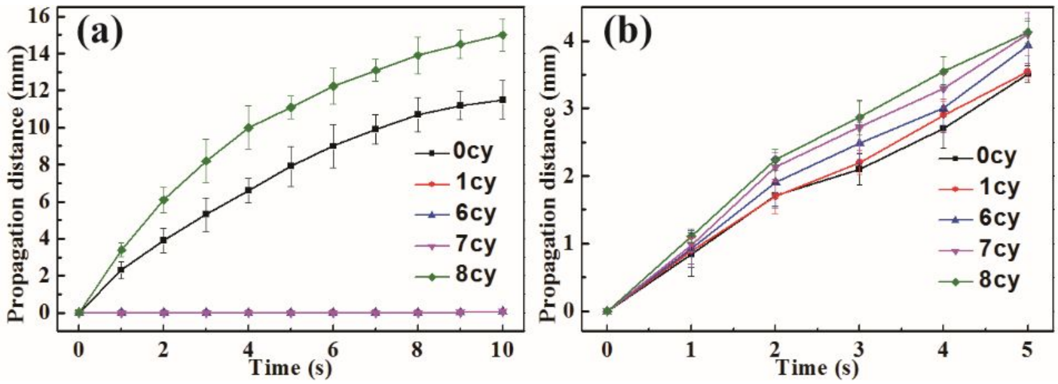

Figure S8 The variation of propagation distance of aerogels as a function of time: (a) water wicking performance and (b) oil wicking performance, demonstrating 8cy-ALD aerogels showed higher water wicking performance than 0cy-ALD aerogels, and all aerogels exhibited good oil wicking performance.

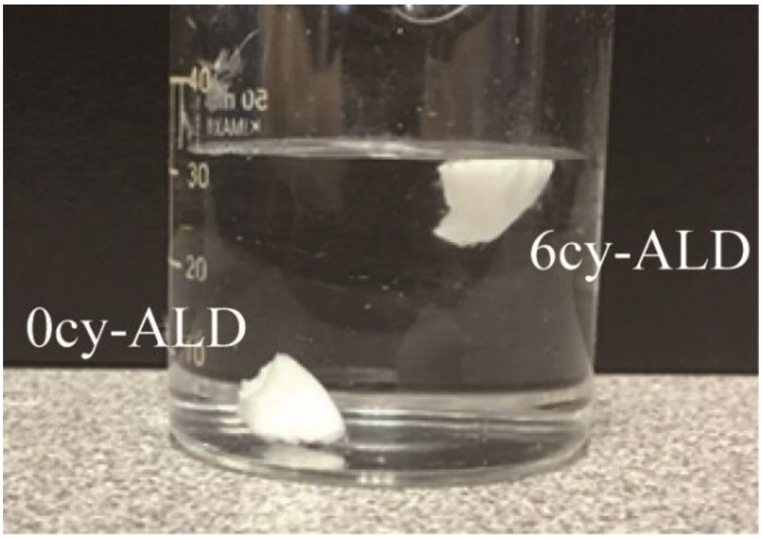

Figure S9 0 and 6cy-ALD aerogels immersed into water after absorption saturation, demonstrating the difference in water absorption between 0 and 6cy-ALD aerogels.

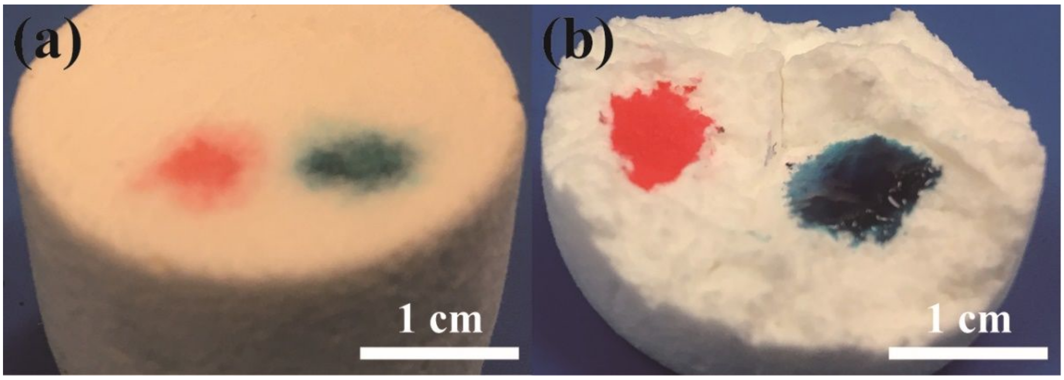

Figure S10 The dyed water droplets on the (a) exterior and (b) interior of 100cy-ALD aerogels, demonstrating both the exterior and interior of 100cy-ALD exhibit hydrophilic.

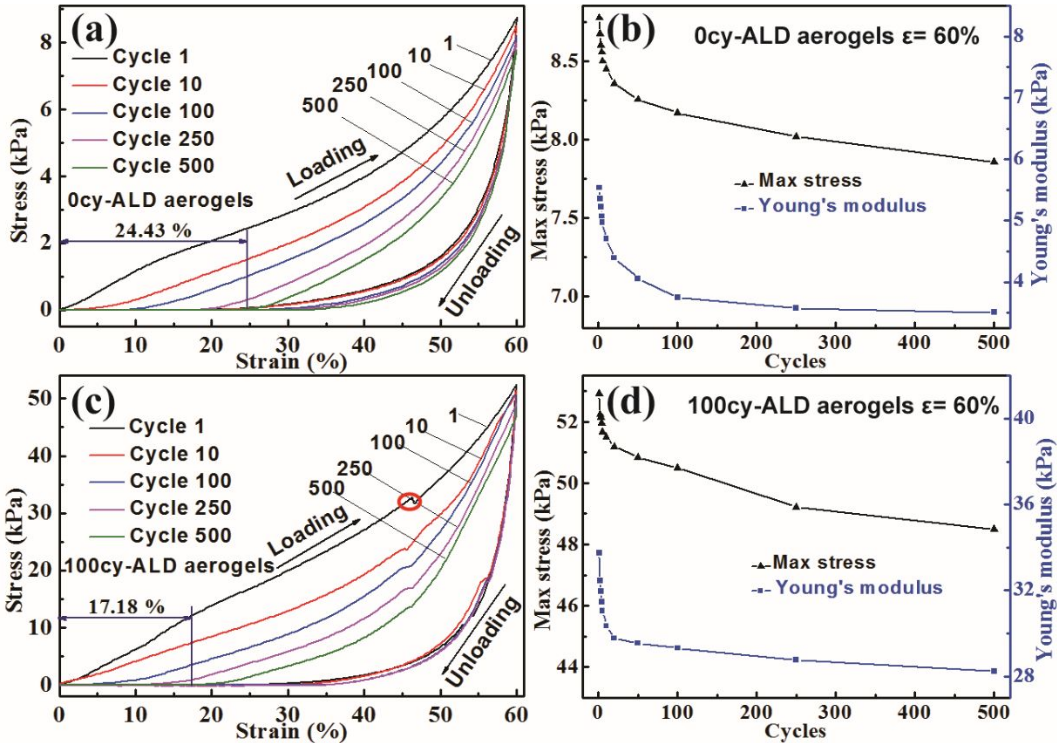

Figure S11 Cyclic stress−strain curves of (a) 0 and (c) 100cy-ALD aerogels with ε of 60%, (b) and (d) the corresponding Young's modulus and maximum stress as a function of the compressive test cycles, demonstrating that 0 and 100cy-ALD aerogels exhibited good mechanical durability and stability.

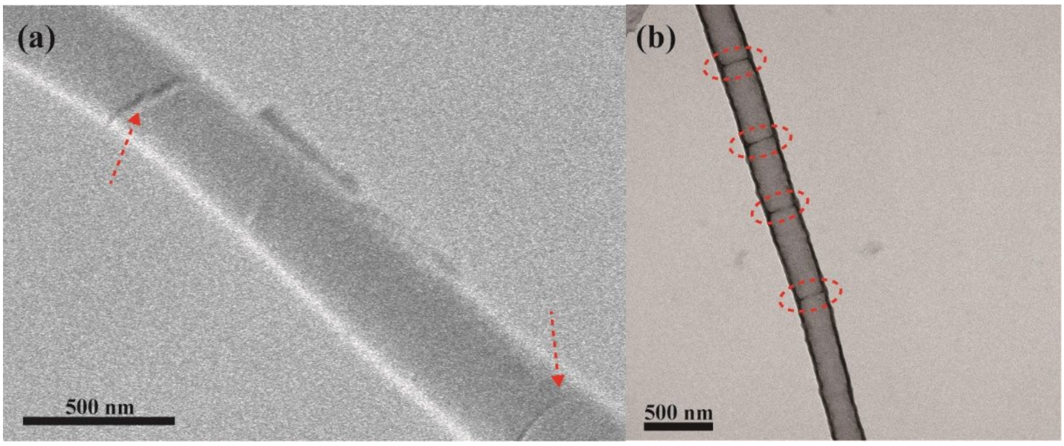

Figure S12 (a) SEM micrograph of a nanofiber, (b) TEM micrograph of a hollow nanotube in 100cy-ALD aerogels after cyclic compression, demonstrating fracture of Al_2O_3 coating on the surface of nanofibers after cyclic compression test.

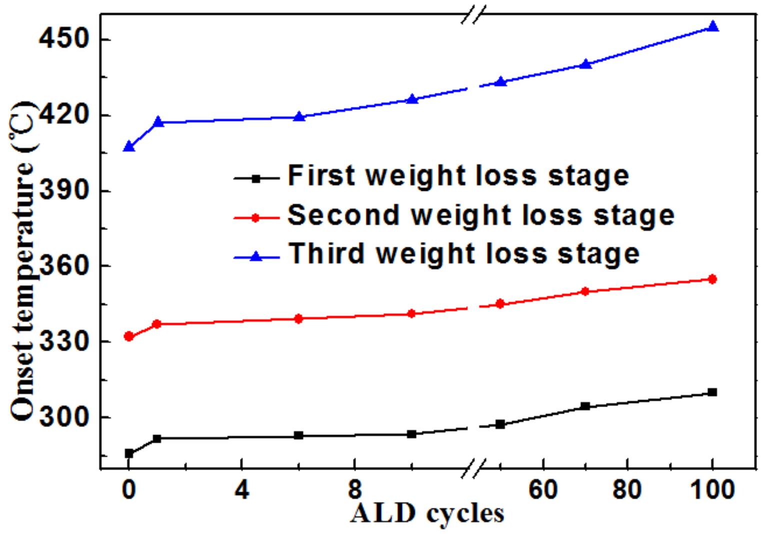

Figure S13 the onset temperature of three weight loss stages of aerogels with various ALD cycles, demonstrating that with increasing cycles of ALD, the thermal stability of aerogels improved.

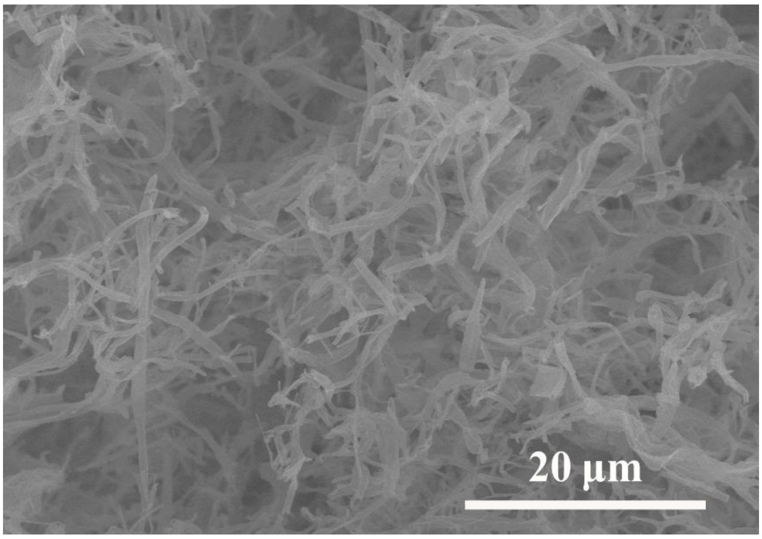

Figure S14 FE-SEM micrograph of Al_2O_3 nanotubes aerogels, the internal porous structure of hollow nanotube aerogels was exhibited, demonstrating good thermal stability of Al_2O_3 nanotubes aerogels

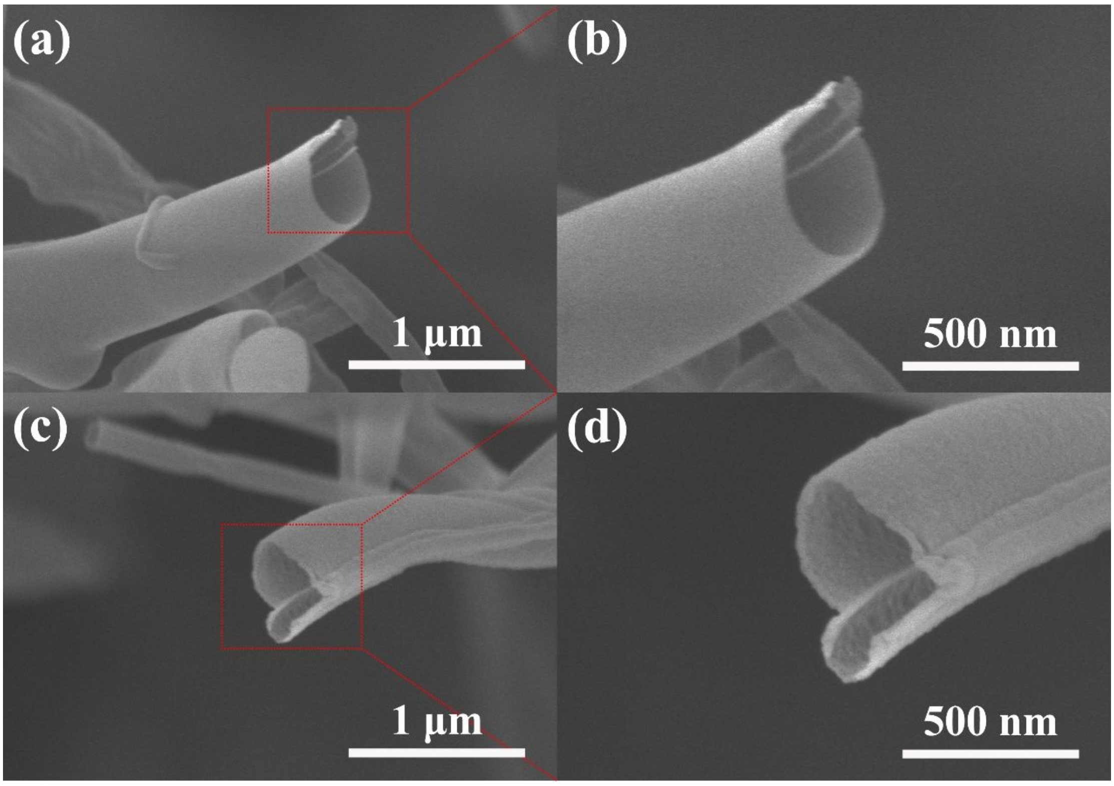

Figure S15 FE-SEM micrographs of 100-cy ALD Al_2O_3 nanotubes (a)surface and (d) buried surface of hollow nanotube aerogels, (b, d) close-ups on Al_2O_3 nanotubes demonstrate their hollow structure.

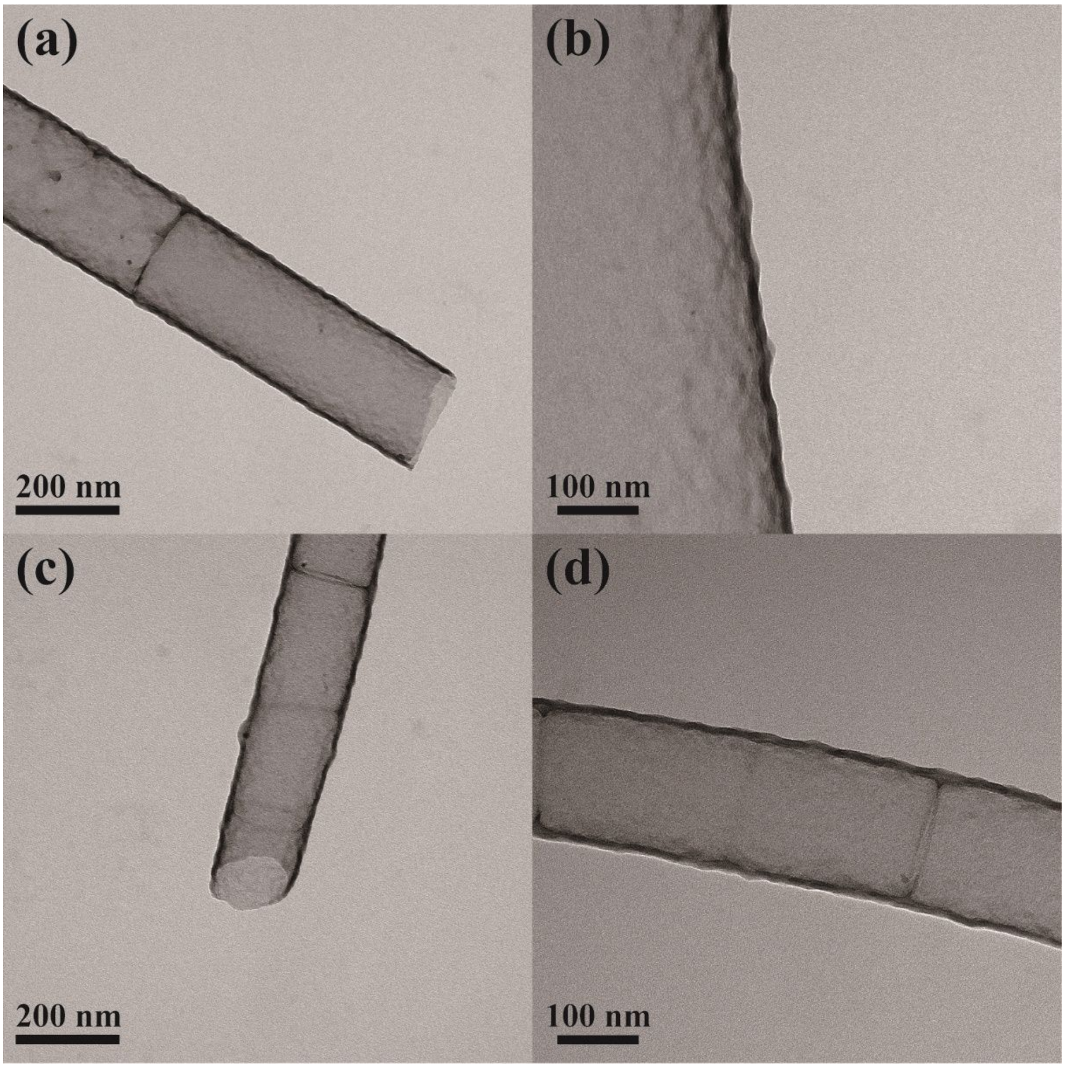

Figure S16 TEM micrographs of the continuous and uniform 100cy-ALD Al_2O_3 coatings of (a, b) surface and (c, d) inner nanotubes of hollow aerogels various magnifications, demonstrating both exterior and interior of aerogels are uniformly coated by Al_2O_3.

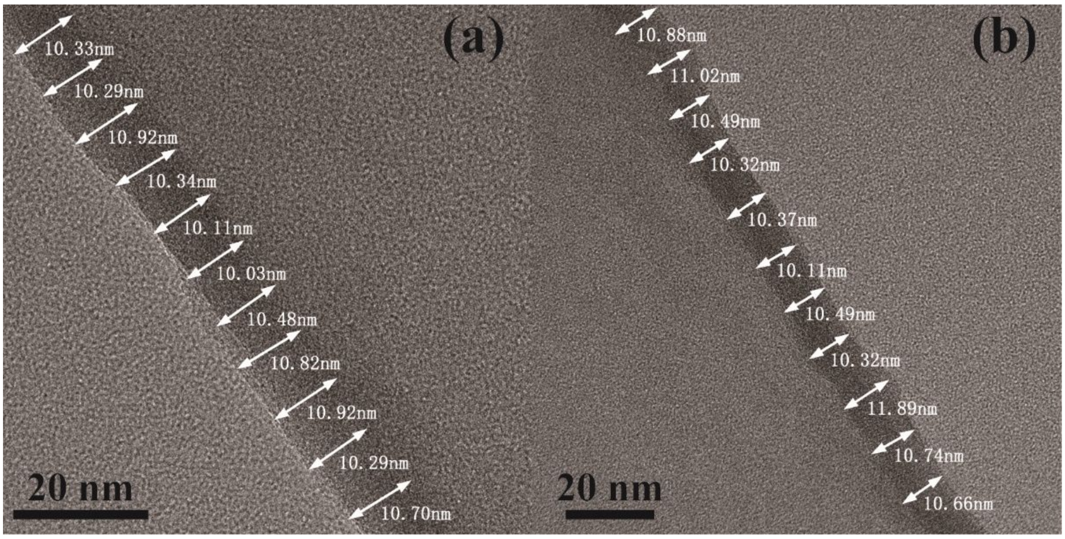

Figure S17 The thickness of 100-cy ALD Al_2O_3 coatings at (a) surface and (b) buried surface of hollow nanotube aerogels, demonstrating the thickness of Al_2O_3 coating inside and outside the aerogels is almost constant.

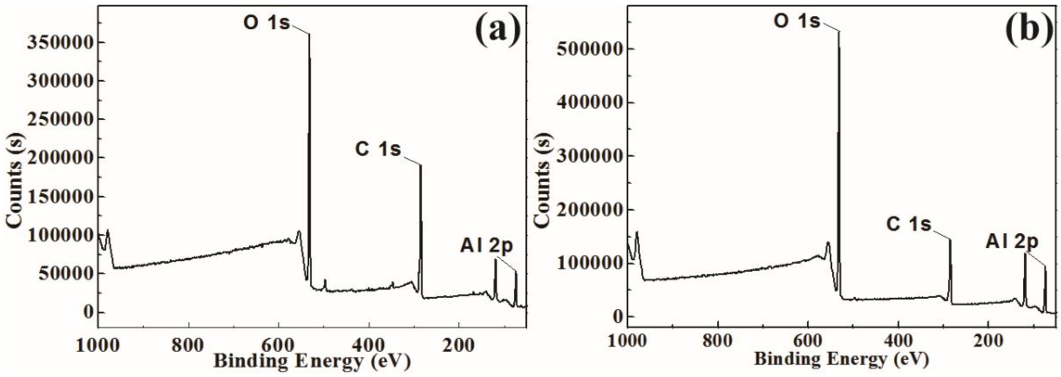

Figure S18 XPS survey scans of 100cy-ALD aerogels before (f) and after (g) pyrolysis, demonstrating that carbon element decreased after pyrolysis.

Table S1 Physical properties of the aerogels with various ALD cycles.

Samples	Mass (mg)	Volume (cm^3)	Density (mg/cm^3)	Porosity (%)	Average pore size (μm)	S_{BET} (m^2/g)
0cy	198.4	12.80	15.50	98.55	3.85	15.96
1cy	199.2	11.64	17.11	98.40	3.37	37.46
6cy	201.3	11.32	17.78	98.35	2.98	44.72
10cy	204.4	11.37	17.98	98.34	2.51	37.96
50cy	214.4	10.97	19.54	98.25	2.42	29.94
70cy	223.7	10.82	20.67	98.20	2.23	20.81
100cy	229.8	10.91	21.06	98.19	2.06	17.68

Table S2 Surface average roughness (R_{sa}) of nanofibers' in 0, 6 and 100cy-ALD aerogels.

Samples	Number	R_{sa} (nm)	R_{sa} of nanofibers (nm)
0cy	1	3.19	2.95
	2	3.01	
	3	2.64	
6cy	1	4.77	4.46
	2	3.96	
	3	4.64	
100cy	1	3.41	3.42
	2	3.63	
	3	3.23	

Table S3 Peak BE and atomic ratio of surface elements and chemical bonds of 0, 1 and 6cy-ALD aerogels.

Samples	Element	Peak BE (eV)	Atomic (%)	Chemical bond	Peak BE (eV)	Atomic (%)
0cy	C 1s	285.32	75.96	C-C/C-H	284.73	64.38
				C-O-C	286.22	27.90
				C=O	287.44	4.99
				O-C=O	288.96	2.74
	O 1s	532.79	24.04	C-O/C=O	532.45	100.00
	Al 2p	-	0	-	-	0
1cy	C 1s	285.24	64.98	C-C/C-H	284.69	64.80
				C-O-C	286.21	27.77
				C=O	287.80	3.74
				O-C=O	289.09	3.69
	O 1s	532.26	29.60	Al-O	531.35	18.59
				C-O/C=O	532.30	81.41
	Al 2p	74.77	5.42	Al-O	74.51	100.00
6cy	C 1s	285.09	68.90	C-C/C-H	284.79	64.80
				C-O-C	286.19	27.77
				C=O	287.61	3.74
				O-C=O	289.01	3.69
	O 1s	532.13	25.14	Al-O	531.44	35.27
				C-O/C=O	532.24	64.73
	Al 2p	74.41	5.96	Al-O	73.74	100.00

Table S4 Peak BE and atomic ratio of surface elements of 100cy-ALD aerogels before and after pyrolysis.

Samples	Element	Peak BE (eV)	Atomic (%)
Before pyrolysis	C 1s	285.17	43.49
	O 1s	531.83	37.74
	Al 2p	74.81	18.77
After pyrolysis	C 1s	285.21	26.10
	O 1s	531.80	46.97
	Al 2p	74.86	26.93

Table S5 Comparison of sorption capacities of various sorbents.

Sorbents	Min sorption capacity (g/g)	Max sorption capacity (g/g)	Density (mg/cm^3)	Porosity (%)	Cost	Reference
PVA-CNF hybrid aerogels	44.56	95.25	13	99.01	Medium	[2]
PVA-co-PE NFA aerogels	23	50	11.1	99	Low	[3]
Cellulose nanofibril aerogels	23	46	23.2	98.5	Low	[4]
Cellulose nanofibril aerogels	65	205	2.9	99.81	Low	[5]
Carbon aerogels	74.22	223.56	7.8	-	Medium	[6]
Polydimethylsiloxane sponge	4	11	180 ~ 750	-	Medium	[7]
Microporous conjugated polymers	6	23	-	-	High	[8]
Cellulose nanofibril aerogels	139	256	1.7~8.1	99.5~99.9	Low	[9]
Carbon nanofiber aerogels	51	139	10	> 99	Medium	[10]
Carbon nanofiber aerogels	106	312	4~6	99.7	Medium	[11]
Carbonaceous fiber aerogel	22	87	36	-	Medium	[12]
Cellulose nanocrystal aerogel	34	99	22.4~23.3	96.3~97.2	High	[13]
Carbon-based aerogels	393	1002	0.7~10.2	99	High	[14]
Melamine sponge	69	176	-	-	Low	[15]
Graphene aerogels	19	26	-	97.6	High	[16]
EVOH nanofibrous aerogels	44.83	101.86	12.3	98.95	Low	[17]
EVOH NFAs coated with Al_2O_3	30.57	73.03	17.78	98.35	Low	Present study

The work mentioned in the paper is defined as the work doing for generating compression deformation per unit volume,[18, 19] which was defined as

$$W = \int_{\varepsilon_1}^{\varepsilon_2} \sigma d\varepsilon \qquad (1)$$

where W is the work, ε_1 and ε_2 are the initial and final compression strain, respectively, and σ is the compression stress. The compression work and recovery work were calculated by the integration of the relevant stress-strain curves. The energy dissipation was the difference of the absolute value of compression work and recovery work.

Movie S1 Dynamic compressive behavior of 6cy-ALD aerogels under a 60% compressive strain. 6cy-ALD aerogels completely recovered their original shape with no mechanical failure after being subjected to 60% strain.

Movie S2 Canola oil was absorbed by 6cy-ALD aerogels. The canola oil dyed with Sudan red III was completely absorbed by 6cy-ALD aerogels in 10 s, the oil-filled aerogels could float on water without any oil release.

Movie S3 Chloroform was absorbed by 6cy-ALD aerogels. 6cy-ALD aerogels could absorb the chloroform dyed with Sudan red III at the bottom of water without water absorption.

REFERENCES

(1) Nguyen, H. M. T.; Tang, H. Y.; Huang, W. F.; Lin, M. C. Mechanisms for Reactions of Trimethylaluminum with Molecular Oxygen and Water. *Comput. Theor. Chem.* **2014**, *1035*, 39-43.

(2) Zheng, Q. F.; Cai, Z. Y.; Gong, S. Q. Green Synthesis of Polyvinyl Alcohol (PVA)-Cellulose Nanofibril (CNF) Hybrid Aerogels and Their Use as Superabsorbents. *J. Mater. Chem. A* **2014**, *2*, 3110-3118.

(3) Liu, Q. Z.; Chen, J. H.; Mei, T.; He, X. W.; Zhong, W. B.; Liu, K.; Wang, W. W.; Wang, Y. D.; Li, M. F.; Wang, D. A Facile Route to the Production of Polymeric Nanofibrous Aerogels for Environmentally Sustainable Applications. *J. Mater. Chem. A* **2018**, *6*, 3692-3704.

(4) Mulyadi, A.; Zhang, Z.; Deng, Y. L. Fluorine-Free Oil Absorbents Made from Cellulose Nanofibril Aerogels. *ACS Appl. Mater. Interfaces* **2016**, *8*, 2732-2740.

(5) Laitinen, O.; Suopajarvi, T.; Osterberg, M.; Liimatainen, H. Hydrophobic, Superabsorbing Aerogels from Choline Chloride-Based Deep Eutectic Solvent Pretreated and Silylated Cellulose Nanofibrils for Selective Oil Removal. *ACS Appl. Mater. Interfaces* **2017**, *9*, 25029-25037.

(6) Chen, W. S.; Zhang, Q.; Uetani, K.; Li, Q.; Lu, P.; Cao, J.; Wang, Q. W.; Liu, Y. X.; Li, J.; Quan, Z. C.; Zhang, Y. S.; Wang, S. F.; Meng, Z. Y.; Yu, H. P. Sustainable Carbon Aerogels Derived from Nanofibrillated Cellulose as High-Performance Absorption Materials. *Adv. Mater. Interfaces* **2016**, *3*, 1-9.

(7) Choi, S. J.; Kwon, T. H.; Im, H.; Moon, D. I.; Baek, D. J.; Seol, M. L.; Duarte, J. P.; Choi, Y. K. A Polydimethylsiloxane (PDMS) Sponge for the Selective Absorption of Oil from Water. *ACS Appl. Mater. Interfaces* **2011**, *3*, 4552-4556.

(8) Li, A.; Sun, H. X.; Tan, D. Z.; Fan, W. J.; Wen, S. H.; Qing, X. J.; Li, G. X.; Li, S. Y.; Deng, W. Q. Superhydrophobic Conjugated Microporous Polymers for Separation and Adsorption. *Energy Environ. Sci.* **2011**, *4*, 2062-2065.

(9) Jiang, F.; Hsieh, Y. L. Amphiphilic Superabsorbent Cellulose Nanofibril Aerogels. *J. Mater. Chem. A* **2014**, *2*, 6337-6342.

(10) Wu, Z. Y.; Li, C.; Liang, H. W.; Zhang, Y. N.; Wang, X.; Chen, J. F.; Yu, S. H. Carbon Nanofiber Aerogels for Emergent Cleanup of Oil Spillage and Chemical Leakage under Harsh Conditions. *Sci Rep.* **2014**, *4*, 4-16.

(11) Wu, Z. Y.; Li, C.; Liang, H. W.; Chen, J. F.; Yu, S. H. Ultralight, Flexible, and Fire-Resistant Carbon Nanofiber Aerogels from Bacterial Cellulose. *Angew. Chem., Int. Ed.* **2013**, *52*, 2925-2929.

(12) Liu, R. L.; Li, X. Q.; Liu, H. Q.; Luo, Z. M.; Ma, J.; Zhang, Z. Q.; Fu, Q. Eco-Friendly Fabrication of Sponge-Like Magnetically Carbonaceous Fiber Aerogel for High-Efficiency Oil-Water Separation. *Rsc Adv.* **2016**, *6*, 30301-30310.

(13) Ma, H. Q.; Wang, S. J.; Meng, F. B.; Xu, X. Y.; Huo, X. L. A Hydrazone-Carboxyl Ligand-Linked Cellulose Nanocrystal Aerogel with High Elasticity and Fast Oil/Water Separation. *Cellulose* **2017**, *24*, 797-809.

(14) Li, C.; Wu, Z. Y.; Liang, H. W.; Chen, J. F.; Yu, S. H. Ultralight Multifunctional Carbon-Based Aerogels by Combining Graphene Oxide and Bacterial Cellulose. *Small* **2017**, *13*, 1-8.

(15) Huang, S. Y.; Li, X.; Jiao, Y. Q.; Shi, J. F. Fabrication of a Superhydrophobic, Fire-Resistant, and Mechanical Robust Sponge upon Polyphenol Chemistry for Efficiently Absorbing

Oils/Organic Solvents. *Ind. Eng. Chem. Res.* **2015**, *54*, 1842-1848.

(16) Ren, R. P.; Li, W.; Lv, Y. K. A Robust, Superhydrophobic Graphene Aerogel as a Recyclable Sorbent for Oils and Organic Solvents at Various Temperatures. *J. Colloid Interface Sci.* **2017**, *500*, 63-68.

(17) Lu, J. W.; Xu, D. D.; Wei, J. K.; Yan, S.; Xiao, R. Superoleophilic and Flexible Thermoplastic Polymer Nanofiber Aerogels for Removal of Oils and Organic Solvents. *ACS Appl. Mater. Interfaces* **2017**, *9*, 25533-25541.

(18) Schaedler, T. A.; Jacobsen, A. J.; Torrents, A.; Sorensen, A. E.; Lian, J.; Greer, J. R.; Valdevit, L.; Carter, W. B. Ultralight Metallic Microlattices. *Science* **2011**, *334*, 962-965.

(19) Si, Y.; Yu, J. Y.; Tang, X. M.; Ge, J. L.; Ding, B. Ultralight Nanofibre-Assembled Cellular Aerogels with Superelasticity and Mmultifunctionality. *Nat. Commun.* **2014**, *5*, 1-9.